Calculation of the second self-diffusion and viscosity virial coefficients of Lennard-Jones fluid by equilibrium molecular dynamics simulations

Hassan Yousefi Oderji, Hongbin Ding, and Hassan Behnejad

Phys. Rev. E **83**, 061202 — Published 16 June 2011

DOI: 10.1103/PhysRevE.83.061202

Calculation of the second self-diffusion and viscosity virial coefficients of the Lennard-Jones fluid by equilibrium molecular dynamics simulations

Hassan Yousefi Oderji,[1,2] Hongbin Ding,[1,*] and Hassan Behnejad[2]

[1] *School of Physics and Optical Electronic Technology, Dalian University of Technology, Dalian, Liaoning 116024, P. R. China*

[2] *Department of Physical Chemistry, School of Chemistry, University College of Science, University of Tehran, Tehran 14155, Iran*

Abstract

The second self-diffusion and viscosity virial coefficients of the Lennard-Jones (LJ) fluid were calculated by a detailed evaluation of the velocity and shear-stress autocorrelation functions using equilibrium molecular dynamics simulations at low and moderate densities. Accurate calculation of these coefficients requires corresponding transport coefficient values with low degrees of uncertainty. These were obtained via very long simulations by increasing the number of particles and by using the knowledge of correlation functions in the Green-Kubo method in conjunction with their corresponding generalized Einstein relations. The values of the self-diffusion and shear viscosity coefficients have been evaluated for systems with reduced densities between 0.0005 and 0.05, and reduced temperatures from 0.7 to 30.0. This provides a new insight into the transport coefficients beyond what can be offered by the Rainwater-Friend theory, which has not been developed for the self-diffusion coefficient.

PACS numbers: 51.10.+y, 05.20.Dd, 61.20.Lc, 66.10.cg, 66.20.-d

* Corresponding author; Tel: +86-411-84706730; Fax: +86-411-84706730; E-mail: hding@dlut.edu.cn

I. INTRODUCTION

Transport coefficients, which are important to many applications, particularly the optimization of chemical processes, depend on temperature and density as well as on the type of fluid. Hence, accurately predicting these coefficients for even simple fluids over a wide range of densities and temperatures has been a matter of much consideration within the field of nonequilibrium statistical mechanics, dating from the Enskog's early work [1, 2]. At present, there are several approaches to the study of transport coefficients; some of them are as follows: the Chapman-Enskog solution of the Boltzmann equation in the kinetic theory for low densities (zero-density limit), the Rainwater-Friend (RF) and modified Enskog theory for moderate densities, and the corresponding states correlation function theory for high densities [3–12]. The time correlation function theory can also be used to calculate the transport coefficients at all densities and temperatures [13].

The second transport virial coefficient may be evaluated as the first density correction of its corresponding transport coefficient. In the 1980s, Rainwater and Friend introduced a theoretical model for the calculation of second transport virial coefficients containing the effects of two-body collisional transfer and both three-monomer and monomer-dimer collisions [7, 8]. This theory is supported by the fact that a real fluid differs from a hard sphere mainly in the temperature dependence of the collision frequency and pressure of the fluid. Rainwater and Friend presented the second viscosity and thermal conductivity virial coefficients for the Lennard-Jones (LJ) potential model [7, 8]. Najafi and co-workers employed the more accurate potential of HFD-type (Hartree-Fock-Dispersion) for noble gases and Behnejad *et al.* used an accurate and realistic Morse-Spline-Van der Waals (MSV) potential model to improve upon the theoretical results produced by the Rainwater and Friend model for real fluids [9–12, 14–16].

The major difficulty in comparing the theoretical results of model fluids with the experimental results is the differences between the model and real Hamiltonians [17]. For this reason, computer simulations of model fluids can be used for assessing theories. In this work, the second virial coefficients of the viscosity and self-diffusion coefficients have been calculated by equilibrium molecular dynamics (EMD) simulations for LJ fluids. The results of the viscosity coefficients have been compared using the Rainwater-Friend theory [8]. To date, the Rainwater-Friend theory has not been extended to the self-diffusion coefficient.

The application of EMD to the calculation of transport properties is well known, but the correct evaluation of the correlation functions used to obtain second transport virial coefficients is a troublesome task. While experimental data generated by Teske and Vogel show that the effect of the second viscosity virial coefficient at densities lower than 0.002 is only 1%, the statistical uncertainties in the simulation results found by Meier *et al.*, who simulated a LJ model fluid in extensive ranges of temperature and density, are more than 10% for the viscosity and 1% for the self-diffusion coefficients at low densities [18–22]. Meier and co-workers stated that reliable results for the second transport virial coefficients could not be given with any reasonable degree of precision. Nevertheless, these researchers explored a possible means of estimating the second self-diffusion virial coefficient as a function of temperature. In addition, at low densities, the density dependence of transport coefficients must be determined by interpolation. To our knowledge, this has not been investigated, so we extended our investigation to the densities as low as 0.0005. As Alder and Wainwright pointed out, the study of autocorrelation functions at low densities made difficult by the fact that the system must be so large that a molecule undergoes many collisions before a sound wave travels across the whole system [23]. Since the correlation functions decay very slowly at low densities, the uncertainty of the values for long correlation times has been discussed in detail. Furthermore, we increased the length of the simulation to 50 times that of previous studies to decrease the likelihood of statistical error, and we increased the number of particles to 2048 to improve the accuracy of the self-diffusion coefficient, which is a single-particle property [20, 21]. The latter is particularly useful because it can decrease the artificial effects of periodic boundary conditions (PBC) on the velocity autocorrelation functions for long correlation times. In addition, a detailed analysis on autocorrelation functions has been performed to evaluate the decay time values, the artificial effects from PBC, and the decay behavior at long correlation time. Finally, the self-diffusion coefficients were calculated using the Einstein approach, in which some of the parameters were determined according to velocity autocorrelation functions, while the shear viscosity coefficients were obtained directly by evaluating shear-stress correlation functions using the Green-Kubo approach [13].

This paper is organized as follows: The next section provides a theoretical background for transport coefficients and presents the details of the simulation. Section III evaluates the behavior of autocorrelation functions. Sections IV and V present the methods and the results for the calculated second self-diffusion and viscosity virial coefficients, respectively.

II. THEORY AND SIMULATION DETAILS

In contrast to thermodynamic properties, transport coefficients cannot be evaluated as a power series of density so that a logarithmic term appears in the series such as the following:

$$X(\rho,T) = X_0(T)\left[1 + B_{\mathrm{X}}\,\rho + C_{\mathrm{X}}\,\rho^2 \ln\rho + D_{\mathrm{X}}\,\rho^2 + \cdots\right], \tag{1}$$

where X is $D\rho$, the self-diffusion coefficient, or η, the shear viscosity coefficient [24]. It should be noted that D is multiplied by ρ to remove the singularity of the self-diffusion coefficients in zero density limit, and, in this paper, $D\rho$ is referred to as self-diffusion for simplicity [1, 3]. B_{D} and B_η are the second self-diffusion and shear viscosity virial coefficients, while C_{X} and D_{X} are higher-order virial transport coefficients. $(D\rho)_0$ and η_0 are the zero density limits of the self-diffusion and viscosity coefficients, which can be obtained by the kinetic theory from the Chapman-Enskog solution of the Boltzmann equation [3].

Evaluation of the second transport virial coefficients requires their corresponding transport coefficients at the low and moderate densities along the desired isotherms. Therefore, 180 state points were selected on the phase diagram of a LJ model fluid with reduced density ranging from 0.0005 to 0.05, and reduced temperatures ranging from 0.7 to 30.0. Reduced quantities are defined as follows: reduced temperature, $T^* = kT/\varepsilon$; reduced shear viscosity coefficient, $\eta^* = \eta\sigma^2/\sqrt{m\varepsilon}$; reduced self-diffusion coefficient, $D^* = D\sqrt{m/\varepsilon}/\sigma$; reduced time, $t^* = t\sqrt{\varepsilon/m}/\sigma$; reduced density, $\rho^* = \rho\sigma^3$, where k is the Boltzmann constant, m is the mass of a particle, and ε and σ are the energy and length scaling parameters for LJ potential as follows:

$$V_{LJ} = 4\varepsilon\left\{\left(\frac{\sigma}{r}\right)^{12} - \left(\frac{\sigma}{r}\right)^{6}\right\}. \tag{2}$$

One of the methods for calculating transport coefficients, which is applicable to all densities and temperatures, is the time correlation function approach, which is a result of the Onsager hypothesis [13, 25]. Using this method, which is based on linear response theory, the self-diffusion coefficient can be calculated using the Green-Kubo integral equation or equivalently via its corresponding Einstein relation:

$$D = \frac{1}{3N}\sum_{i=0}^{N}\int_0^\infty \langle \mathbf{v}_i(t)\cdot\mathbf{v}_i(t_0)\rangle\, dt, \tag{3}$$

$$D = \lim_{t\to\infty}\frac{1}{6N}\sum_{i=1}^{N}\frac{d}{dt}\left\langle[\mathbf{r}_i(t) - \mathbf{r}_i(t_0)]^2\right\rangle, \tag{4}$$

where N is the number of particles, $\mathbf{r}_i$ and $\mathbf{v}_i$ are the position and velocity vectors of particle i, respectively, and t is time [26]. The angular brackets indicate ensemble averaging over short sub-trajectories of the system with time origin, t_0. In both relations, averaging is over all particles to reduce likelihood of statistical error. Similarly, the shear viscosity coefficients can be calculated using the Green-Kubo integral equation or equivalently using its corresponding Einstein relation as follows:

$$\eta = \frac{V}{kT} \int_0^\infty \langle \tau_{\alpha\beta}(t) \tau_{\alpha\beta}(t_0) \rangle \, dt, \tag{5}$$

$$\eta = \frac{V}{2kT} \lim_{t\to\infty} \frac{d}{dt} \left\langle \left[\frac{m}{V} \sum_{i=1}^{N} \left[v_{i,\alpha}(t) r_{i,\beta}(t) - v_{i,\alpha}(t_0) r_{i,\beta}(t_0) \right] \right]^2 \right\rangle, \tag{6}$$

where, V stands for the volume of the primary cell, $\tau_{\alpha\beta}$ denotes an off-diagonal element of the stress tensor, $v_{i,\alpha}$ and $r_{i,\beta}$ are the Cartesian components of the velocity and position for particle i ($\alpha, \beta = x, y, z; \alpha \neq \beta$). In order to decrease likelihood of statistical error, averaging is performed over all independent tensor elements e.g., τ_{xy}, τ_{xz}, τ_{yz}; $\tau_{\alpha\beta}$ is related to phase space variables of simulated system as follows:

$$\tau_{\alpha\beta} = -\frac{1}{V} \sum_{i=1}^{N} m v_{i,\alpha} v_{i,\beta} - \frac{1}{V} \sum_{i=1}^{N-1} \sum_{j=i+1}^{N} r_{ij,\alpha} f_{ij,\beta}, \tag{7}$$

in which $f_{ij,\beta}$ is β component of the force vector and $r_{ij,\alpha}$ is the α component of the distance vector between particles i and j [27]. The instant positions and velocities of particles can be obtained by EMD simulations; the accuracy depends on the integration algorithm and simulation parameters. In this work, we used optimized simulation parameters to decrease the rate of computational error and improve the required statistical precision for evaluating the second virial transport coefficients. The systems were equilibrated 5×10^6 and simulated 1×10^8 time-steps for the low density, and 1×10^6 and 5×10^7 for the moderate density states by the DL_POLY molecular dynamics parallel simulation package in NVE ensemble with 2048 LJ particles in the primary cell under the cubic periodic boundary conditions and sampled at every 50th time-step for the positions and velocities of all particles as well as at the every time-step for the independent off-diagonal elements of the stress tensor [28]. The time-step length (Δt^*) and the potential cutoff radius parameters were selected as 0.0023 and 6.75 in the reduced units, respectively. The Lennard-Jones potential model was used to compare the simulated results to the values of the second viscosity virial coefficients from

the Rainwater-Friend theory [8]. NVE is the intrinsic ensemble of EMD, so it produces much realistic phase space trajectories at longer time periods. However, using this ensemble leads to small differences between the simulated and the desired temperatures, but these can be accounted for by applying a proper temperature correction. Equilibrium status of the systems was checked by comparing the averaged configuration energy, temperature and pressure values in two different intervals from the initial and final parts of the simulated trajectories. Moreover, the results of this examination confirm the stability of the velocity-Verlet integrator for a LJ system even for very long simulations.

III. EVALUATION OF THE AUTOCORRELATION FUNCTIONS

The self-diffusion coefficient is related to the velocity autocorrelation function integral as in Eq. (3) and the shear viscosity is related to the off-diagonal elements of the stress tensor correlation function as in Eq. (5). Hence, the study of these functions is useful for the more accurate calculation of the corresponding transport coefficients. First, the presence or absence of the long-time tail for correlation functions was examined to assess the accumulation of computational errors at long times.

Velocity autocorrelation function (VACF), $\langle \mathbf{v}(t) \cdot \mathbf{v}(t_0) \rangle$, shows how the present velocity of a particle is related to its previous value and how that effects its subsequent velocities. According to the Boltzmann-Enskog theory and the macroscopic Langevin relation, VACF decays exponentially, but Alder and Wainwright found a power decay at the long correlation time using EMD simulations of 500 hard spheres particles at a reduced density of 0.47 and found that VACF decays as $t^{-d/2}$ in the long term, where d is the dimension of the simulated system [23, 29, 30]. Recently, Isobe revisited the 2D long-time tail problem with 1×10^6 particles and performed a large-scale, long-time, statistically accurate EMD simulation and found that, in moderately dense fluids, VACF decays slightly faster than $\sim 1/t$ [31]. This is in accordance with the prediction of the self-consistent mode-coupling theory in the long-time limit, $\sim 1/t\sqrt{\ln t}$ [32, 33]. At long correlation times, the power decay of VACF, rather than the exponential decay, is related to the domination of the transverse hydrodynamic mode to the longitudinal mode in the dissipation of particle momentum over long periods of time.

Nevertheless, the longitudinal hydrodynamics mode in the momentum dissipation, which

propagates through the periodic boundary conditions, can reflect the artificial correlations at long time and should be considered in the study of very slow decaying correlation functions, such as those used in the present project. The maximum value of time, $t_{\max}$, in which the error from the artificial effect of PBC on the correlations is not important, can be related to the length of the simulation cell by $t_{\max} = L/c_{\rm s} = 1/c_{\rm s}(N/\rho)^{1/3}$, where $c_{\rm s}$ is the speed of sound. Here, we used the following equation to calculate $c_{\rm s}$ from EMD simulation as follows:

$$c_{\rm s} = \sqrt{\frac{1}{\rho m \kappa_{\rm s}}}, \tag{8}$$

where, m is the atomic mass, and $\kappa_{\rm s}$ is the adiabatic compressibility, which is calculated for LJ systems as follows:

$$\kappa_{\rm s}^* = \frac{\kappa_{\rm s}\varepsilon}{\sigma^3} = \left[7P^* - \frac{16\rho^* T^*}{3} - 8\rho^* U_{\rm c}^* - \frac{N}{\rho^* T^*}\left\langle (\delta P^*)^2 \right\rangle\right]^{-1} \tag{9}$$

where, $U_{\rm c}^*$ is the reduced internal energy per atom [34]. Table I shows adiabatic compressibility, the speed of sound, and $t_{\max}$ values for systems with particle numbers from 108 to 4000, simulated for the duration of $t^* = 1 \times 10^8$ at $T^* = 1.2$ and $\rho^* = 0.001$. It is worthwhile to note that the number of particles has no significant effect on $\kappa_{\rm s}^*$, so $t_{\max}$ increases as the cubic root of the number of atoms does.

In the other hand, common numerical calculation errors and errors from approximations in the integration algorithms can accumulate over longer correlation times, and their effects become intensified. Averaging over numerous statistical samples can reduce these errors. Furthermore, to improve the statistical precision, every simulated trajectory can be divided into many sub-trajectories, or time windows, in which the correlation functions decay to zero [35]. The time interval between two successive time windows, $t_{\rm o}^*$, and the time interval between two successive sampling from the simulated trajectory, $t_{\rm s}^*$, can be optimized to save CPU time. For the system with 1372 particles at a reduced density of 0.05 and a reduced temperature of 1.0 simulated for the duration of $t^* = 14000$, Figure 1 shows that the curves of VACFs for $t_{\rm s}^* = \Delta t^*$ (square symbol) and $t_{\rm s}^* = 500\Delta t^*$ (circle symbol) are the same. Furthermore, these results indicate an unspecified deviation from exponential decay over long periods of time. This seems due to the finite size effects, so, according to Alder and Wainwright and, more recently, Naitoh *et al.*, we applied a correction on VACF by adding a constant correction term, $1/(N-1)$, to the results of simulation with 1372 particles [23, 36]. This is based on the theory of conservation of momentum: whenever

one particle has a velocity v, the average velocity of other particles should be $-v/(N-1)$. Subsequently, the corrected results (represented by a diamond symbol) are compatible with the results (represented by a triangle symbol) from the simulation of a system with 2048 particles at the same density and temperature. Figure 1 shows that both correlations from the simulation of 2048 particles during $t^* = 4.6\times10^3$ and corrected correlations obtained from the simulation of 1372 particles demonstrate a power decay. This long-time tail, however, seems to disappear when the length of the simulation is extended from $t^* = 4.6 \times 10^3$ to $t^* = 1.4 \times 10^5$. Thus, for systems with 2048 particles at various densities and temperatures, such as the one in the present work, the long-time tail has not been found to have correlation time values less than t^*_{max}. Similarly, the effect of t^*_{o} on shear-stress correlations has been examined for the system with a reduced density of 0.01 and a reduced temperature of 5.0 with sampling performed at every step and a simulation of $t^* = 2.3 \times 10^5$ in duration. Figure 2 demonstrates that there are no significant differences for the correlation values when t^*_{o} is less than $500\Delta t^*$. In addition, a comparison of Figure 1 to Figure 2 indicates that the uncertainty in the velocity autocorrelation values is in the order of 10^{-4} while for the normalized shear-stress correlations, the uncertainty is in the order of 10^{-3}. Thus, it can be concluded that the self-diffusion coefficients can be obtained much accurately.

IV. CALCULATION OF SECOND SELF-DIFFUSION VIRIAL COEFFICIENTS

In order to calculate the self-diffusion coefficients precisely, we used both the knowledge obtained from Green-Kubo evaluation of VACF and the Einstein approach. The Einstein approach is preferred because the velocity-Verlet integrator computes the positions more accurate than the velocities, and the evaluation of VACF is useful because it gives the lowest physically infinite time in Eq. (4) [27]. This mixed method can avoid the errors that would arise on the mean-squared displacement (MSD) curves if a linear regime were to be used. Moreover, the self-diffusion coefficient is a single-particle property, so it can be averaged out over all particles to increase statistical accuracy. In practice, at each state point, we calculated the values of $D^*\rho^*$ as a function of the correlation time by measuring the instant slope of MSD for all particles, and then we averaged the values beyond decay time in the VACF curves. Figure 3 shows the typical $D^*\rho^*$ variations versus the time of correlation for a system with a reduced temperature of 1.8 and a reduced density of 0.02.

There are only small variations around the mean value. Thus, the standard deviations are small and it is possible to calculate the self-diffusion coefficient values to a high level of precision using the simulation parameters described in this work.

In order to calculate MSD and VACF curves, the order-n algorithm was used because it can be adjusted to the sampling parameters. This makes it applicable for computing both the slow and fast correlation decays simultaneously, namely the low- and high-density systems. In this algorithm, the block sums of the velocities are first calculated and saved in distinct time intervals, and then the values of the velocities are determined at the desired times by using a recursive relation between the values of the subsequent block sums. More details about this algorithm can be found in Ref. [37].

The values of the self-diffusion coefficients and their standard deviations are presented in Table I in the Supplementary Information section [38]. The values at zero density limit are calculated from the Chapman-Enskog theory [3]. For isotherms of 0.7, 0.8, and 0.9, the systems are metastable at densities higher than 0.015, 0.03, and 0.045, respectively, so the temperature values of these systems change toward the nearest stable states due to adjustment of temperature in the NVE ensemble during the equilibration stage.

While the calculation of the second self-diffusion virial coefficients necessarily involves a survey of the self-diffusion density dependence along specified isotherms (FIG. 4), the self-diffusion coefficient values are related to the simulated temperatures, which are somewhat different from the desired temperatures. Because the standard deviations of the calculated self-diffusion coefficients are very low, it is useful to have a temperature correction on them to adjust their values for the desired isotherms. The differences between the simulated ($T^*_{\rm sim}$) and the desired temperatures ($T^*_{\rm des}$) are small, so a first-order Taylor series in terms of the reduced temperature can be used to predict $D^*\rho^*$ at $T^*_{\rm des}$ as follows:

$$D^*\rho^*\left(\rho^*, T^*_{\rm des}\right) = D^*\rho^*\left(\rho^*, T^*_{\rm sim}\right) + \left(T^*_{\rm des} - T^*_{\rm sim}\right)\frac{\Delta D^*\rho^*\left(\rho^*, T^*_{\rm sim}\right)}{\Delta T^*} \tag{10}$$

where the first derivative is approximated from the difference between $D^*\rho^*$ at $T^*_{\rm sim}$ and $D^*\rho^*$ at the nearest simulated temperature to $T^*_{\rm des}$ along an isochore. The values at $T^*_{\rm sim}$ are shown as the unfilled circles and the corrected values are shown as the filled squares with error bars in Figures 4(a) and 4(b). These figures show the density dependence of the reduced self-diffusion coefficients divided by their values at the zero density limit that is calculated from the Chapman-Enskog theory at the different temperatures. The results

indicate that it is possible to approximate the values of the self-diffusion coefficients as the first order power series of density, as in Eq. (1), within the density ranges covered in this project, so we calculated the second self-diffusion virial coefficients as the slope of solid straight lines in FIG. 4(a) and in FIG. 4(b) up to the reduced temperature of $T^* = 5.0$. At higher temperatures, it seems that higher order terms in Eq. (1) are not negligible. Thus, the isotherms of $T^* = 8.0$, $T^* = 20.0$ and $T^* = 30.0$ can be fitted to Eq. (1) up to the fourth virial coefficients (dotted line in FIG. 5). This also indicates the importance of the logarithmic term in Eq. (1) by which it becomes possible to give a suitable fit.

The values of the second self-diffusion virial coefficient at different temperatures and their standard deviations are presented in Table II. The thermal behavior of them is also shown graphically in Figure 6 and compared with the approximated values reported by Meier *et al.* [20]. The differences are from 12% up to 35%. The overall thermal behavior of the second self-diffusion virial coefficient is similar to the thermal behavior of the second viscosity and thermal conductivity virial coefficient predicted by the Rainwater-Friend theory [8].

V. CALCULATION OF THE SECOND VISCOSITY VIRIAL COEFFICIENTS

Since the shear viscosity coefficient is a collective property, increasing the number of particles should not have any significant effect on increasing the statistical precision. Nevertheless, to explore it precisely, we performed a set of simulations at a stated point with a reduced density of 0.001 and a reduced temperature of 1.2 by different numbers of particles in the primary simulation cell. In all cases, the simulation length was $t^* = 2.3 \times 10^5$ and other parameters were given as in section II. Figure 7 shows the results of the normalized shear-stress correlation function for these systems. Small deviations in these curves, which grow with time, cannot be attributed to the number of particles because there is no linear relation between them. For example, the curves corresponding to 108 and 4000 particles coincide with each other, and the small deviations between other curves are due to temperature variation and computational errors.

In contrast to the self-diffusion, the viscosity coefficient is not averaged over all particles, so it is obtained with less statistical precision at the same simulation length. Therefore, confidently determining a linear regime in the generalized mean-squared displacement functions as in the Einstein approach shown in Eq. (6) is difficult. Moreover, this approach cannot

be applied directly because the particles trajectories are not continuous in a system that is simulated under periodic boundary conditions. In this work, we used the Green-Kubo approach as described in Eq. (5) to calculate the shear viscosity coefficients. In practice, at every state point, we calculated the values of η^* as a function of time by integrating the shear-stress correlation function and then we averaged the values beyond its decay time. The variations around mean values of the calculated viscosity coefficients (FIG. 8) are higher than the variations around mean values of the calculated self-diffusion coefficients (FIG. 3) when all simulation parameters are equal.

The values of the reduced viscosity coefficients and their standard deviations are presented in Table I of the Supplementary Information section. The values at zero density limit are calculated using the Chapman-Enskog theory [3]. As with self-diffusion, shear viscosity coefficient values are related to the simulated temperatures, which are somewhat different from the desired temperatures, so they can be corrected by using the first-order Taylor series in terms of the reduced temperature, as in Eq. (10), for the self-diffusion coefficient, to obtain η^* at T^*_{des}.

Figures 9(a) and 9(b) show the density dependence of the reduced-viscosity coefficients divided by their values at zero density limit at different temperatures. Although the consistency between viscosities is less than the self-diffusion coefficients, nevertheless, it is possible to approximate their values as the first order power series of density, as in Eq. (1). Thus, the second viscosity virial coefficients can be calculated as the slope of the solid straight lines in Figures 9(a) and 9(b) for all isotherms. The values of the second viscosity virial coefficient at different temperatures and standard deviations are presented in Table II. Figure 10 compares the second viscosity virial coefficients calculated in this work with those reported by the Rainwater-Friend theory at different temperatures. The figure indicates that for temperatures beyond $T* = 1.0$ the simulated B^*_η values are appropriately described by the Rainwater-Friend theory. However, for the reduced temperatures of 0.8, 0.9, and 1.0, the simulated values are higher than the values from the Rainwater-Friend theory and for $T^* = 0.7$, uncertainty in the simulated value is too high to permit a strong statement.

VI. CONCLUSION

The effect of second transport virial coefficients is very small at low densities, so it can be hidden by common simulation errors. This makes it difficult to calculate second transport virial coefficients using common simulation methods. This is why calculation of the second virial transport coefficients requires highly accurate, consistent data for the corresponding transport coefficients in the low and moderate densities. In the present work, we reduced simulation errors by performing very long equilibrium molecular dynamics simulations using optimized parameters. We also evaluated the correlation functions to remove the artificial effects of periodic boundary conditions on the results. Standard deviations of the self-diffusion coefficients obtained in this work are small, so it is possible to extract the second self-diffusion virial coefficients from the data. The results also indicate that even at the high reduced temperatures of 20.0 and 30.0, at which the linear regime cannot be observed, the density expansion with logarithmic terms, as in Eq. (1), can be established. Although, the standard deviations of the simulated viscosity coefficients are not so low as the standard deviations of the self-diffusion coefficients, it is still possible to extract the second viscosity virial coefficients with only reasonable levels of uncertainty. The comparison of the second viscosity virial coefficient with the results of the Rainwater-Friend theory shows that they are compatible beyond $T^* = 1.0$ in the error bars, but at this and lower temperatures the simulated values are higher than the values from RF theory.

ACKNOWLEDGMENTS

This work was supported by the Scientific and Technical Foundation of Liaoning Province (No. 20082168) and by the National Science Foundation of China (No.10875023), Scientific and Technical Key Project (No. 108034) and PhD research program (No. 200801411040) of the Educational Ministry and National Magnetic Confinement Fusion Science Program of China (Nos. 2009GB106004, 2008CB717801). The authors gratefully acknowledge support from the Research Council of Tehran University and the Plasma Physics Computational Center of Dalian University of Technology. HY is in acknowledgment of the Chinese Schol-

arship Council and Dr. Foroutan, Dr. Sun, and Dr. Liu for their help.

---

[1] J. Millat, J. H. Dymond, and C. N. de Castro, *Transport Properties of Fluids: their Correlation, Estimation and Prediction* (Cambridge University Press, Cambridge, England, 1996).

[2] D. Enskog and K. Sven, Vetenskapsakad. Handl **63**, 1 (1922).

[3] J. O. Hirschfelder, C. F. Curtiss, and R. B. Bird, *The Molecular Theory of Gases and Liquids*, revised ed. (Wiley-Interscience, New York, 1964).

[4] D. G. Friend and J. C. Rainwater, Chemical Physics Letters **107**, 590 (1984).

[5] H. J. M. Hanley and E. G. D. Cohen, Physica A: Statistical and Theoretical Physics **83**, 215 (1976).

[6] H. J. M. Hanley, R. D. McCarty, and E. G. D. Cohen, Physica **60**, 322 (1972).

[7] J. C. Rainwater, The Journal of Chemical Physics **81**, 495 (1984).

[8] J. C. Rainwater and D. G. Friend, Phys. Rev. A **36**, 4062 (1987).

[9] H. Behnejad and M. S. Miralinaghi, Journal of Molecular Liquids **113**, 143 (2004).

[10] H. Behnejad and A. Pedram, Chemical Physics **325**, 351 (2006).

[11] B. Najafi, R. Araghi, J. C. Rainwater, S. Alavi, and R. F. Snider, Physica A: Statistical Mechanics and its Applications **275**, 48 (2000).

[12] B. Najafi, Y. Ghayeb, J. C. Rainwater, S. Alavi, and R. F. Snider, Physica A: Statistical and Theoretical Physics **260**, 31 (1998).

[13] R. Zwanzig, Annual Review of Physical Chemistry **16**, 67 (1965).

[14] R. A. Aziz, The Journal of Chemical Physics **99**, 4518 (1993).

[15] T. Hosseinnejad and H. Behnejad, Fluid Phase Equilibria **263**, 85 (2008).

[16] A. Maghari, H. Behnejad, and F. Nematbakhsh, Journal of the Physical Society of Japan **68**, 2276 (1999).

[17] K. M. Dyer, B. M. Pettitt, and G. Stell, The Journal of Chemical Physics **126**, 034502 (2007).

[18] V. Teske and E. Vogel, Journal of Chemical & Engineering Data **51**, 628 (2006).

[19] K. Meier, A. Laesecke, and S. Kabelac, International Journal of Thermophysics **22**, 161 (2001).

[20] K. Meier, A. Laesecke, and S. Kabelac, The Journal of Chemical Physics **121**, 9526 (2004).

[21] K. Meier, A. Laesecke, and S. Kabelac, The Journal of Chemical Physics **121**, 3671 (2004).

[22] K. Meier, A. Laesecke, and S. Kabelac, The Journal of Chemical Physics **122**, 014513 (2005).

[23] B. J. Alder and T. E. Wainwright, Phys. Rev. A **1**, 18 (1970).

[24] J. R. Dorfman, T. R. Kirkpatrick, and J. V. Sengers, Annual Review of Physical Chemistry **45**, 213 (1994).

[25] L. Onsager, Phys. Rev. **37**, 405 (1931).

[26] D. J. Evans and G. P. Morriss, *Statistical mechanics of nonequilibrium Liquids*, 2nd ed. (Cambridge University Press, Cambridge, 2008).

[27] M. P. Allen and D. J. Tildesley, *Computer Simulation of Liquids*, Oxford science publications (Oxford University Press, USA, 1989).

[28] W. Smith and T. R. Forester, Journal of Molecular Graphics **14**, 136 (1996).

[29] P. Resibois and M. De Leneer, *Classical Kinetic Theory of Fluids* (John Wiley & Sons Inc, New York, 1977).

[30] B. J. Alder and T. E. Wainwright, Phys. Rev. Lett. **18**, 988 (1967).

[31] M. Isobe, Phys. Rev. E **77**, 021201 (2008).

[32] K. Kawasaki, Physics Letters A **34**, 12 (1971).

[33] T. E. Wainwright, B. J. Alder, and D. M. Gass, Phys. Rev. A **4**, 233 (1971).

[34] J. M. Haile, *Molecular Dynamics Simulation: Elementary Methods*, 1st ed. (John Wiley & Sons, Inc., New York, NY, USA, 1992).

[35] D. C. Rapaport, *The Art of Molecular Dynamics Simulation*, 2nd ed. (Cambridge University Press, Cambridge, 2004).

[36] T. Naitoh, M. H. Ernst, M. A. van der Hoef, and D. Frenkel, Phys. Rev. A **44**, 2484 (1991).

[37] D. Frenkel and B. Smit, *Understanding Molecular Simulation: From Algorithms to Applications*, 2nd ed., Computational Science Series, Vol. 1 (Academic Press, San Diego, 2001).

[38] See EPAPS Document No.[] for all simulated self-diffusion and viscosity coefficients, and standard deviations at different densities.

FIGURE CAPTIONS:

FIG. 1. Effects of sampling parameter, t_s^*; number of particles, N; length of simulation; and $1/(N-1)$ correction on the velocity autocorrelation function of LJ fluid at reduced density of 0.05 and reduced temperature of 1.0.

FIG. 2. Effect of time interval between the beginnings of two successive time windows, t_o^*, on calculation of the normalized shear-stress correlation function of LJ fluid at a reduced density of 0.01 and a reduced temperature of 5.0.

FIG. 3. Reduced self-diffusion coefficient of LJ fluid at a reduced temperature of 1.8 and a reduced density of 0.02 versus time of correlation (a) from zero-time and (b) from decay-time. (Dotted line: mean value.)

FIG. 4. Density dependence of the simulated reduced self-diffusion coefficients of LJ fluid divided by their values at zero density limit from the Chapman-Enskog theory (a) for isotherms of 0.7 to 1.5 and (b) for isotherms of 1.8 to 5.0. (Filled squares with error bars: temperature corrected values; circles: values at simulated temperatures; solid line: fitted linear regime.)

FIG. 5. Density dependence of the simulated reduced self-diffusion coefficients of LJ fluid divided by their values at zero density limit from the Chapman-Enskog theory for isotherms of 8.0, 20.0, and 30.0. (Legend as in FIG. 4; dotted line: fitted up to fourth term of Eq. (1).)

FIG. 6. Second self-diffusion virial coefficients of LJ fluid as a function of reduced temperature. (Circles with error bars: this work; crosses: from Ref. [20].)

FIG. 7. Normalized shear-stress correlation functions of LJ fluid at a reduced temperature of 1.2 and a reduced density of 0.001 with different numbers of atoms in the simulation primary cell.

FIG. 8. Reduced viscosity coefficient of LJ fluid at a reduced temperature of 1.8 and a reduced density of 0.02 versus time of correlation (a) from zero-time and (b) from decay-time. (Dotted line: mean value.)

FIG. 9. Density dependence of the simulated reduced viscosity coefficients of LJ fluid divided by their values at zero density limit from the Chapman-Enskog theory (a) for isotherms of 0.7 to 2.0 and (b) for isotherms of 2.5 to 30.0. (Legend as in FIG. 4)

FIG. 10. Second viscosity virial coefficients of LJ fluid as a function of reduced temperature. (Circles with error bars: this work; solid line: Rainwater-Friend theory, Ref. [8].)

TABLE CAPTIONS:

TABLE I. Reduced adiabatic compressibility, $\kappa_{\rm s}^*$; reduced speed of sound, $c_{\rm s}^*$; and reduced beginning time of the artificial PBC effect on VACF, $t_{\rm max}^*$, for LJ fluid at $T^* = 1.2$ and $\rho^* = 0.001$, simulated with N particles for the duration of $t^* = 1 \times 10^8$.

TABLE II. Simulated reduced second self-diffusion virial coefficients, $B_{\rm D}^*$; reduced second viscosity virial coefficients, B_η^*; and their standard deviations [$SD(B_{\rm D}^*)$ and $SD(B_\eta^*)$] for the Lennard-Jones fluid at different temperatures.

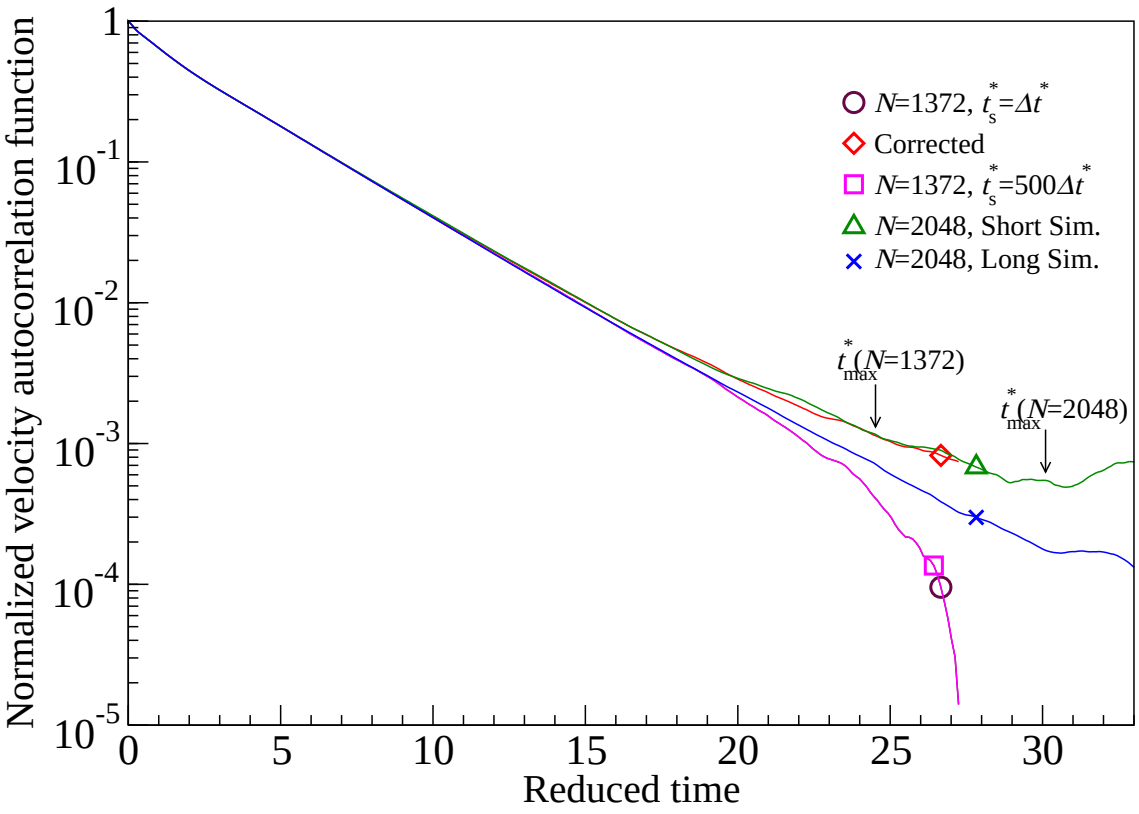

FIG. 1. Effects of sampling parameter, t_s^*; number of particles, N; length of simulation; and $1/(N-1)$ correction on the velocity autocorrelation function of LJ fluid at reduced density of 0.05 and reduced temperature of 1.0.

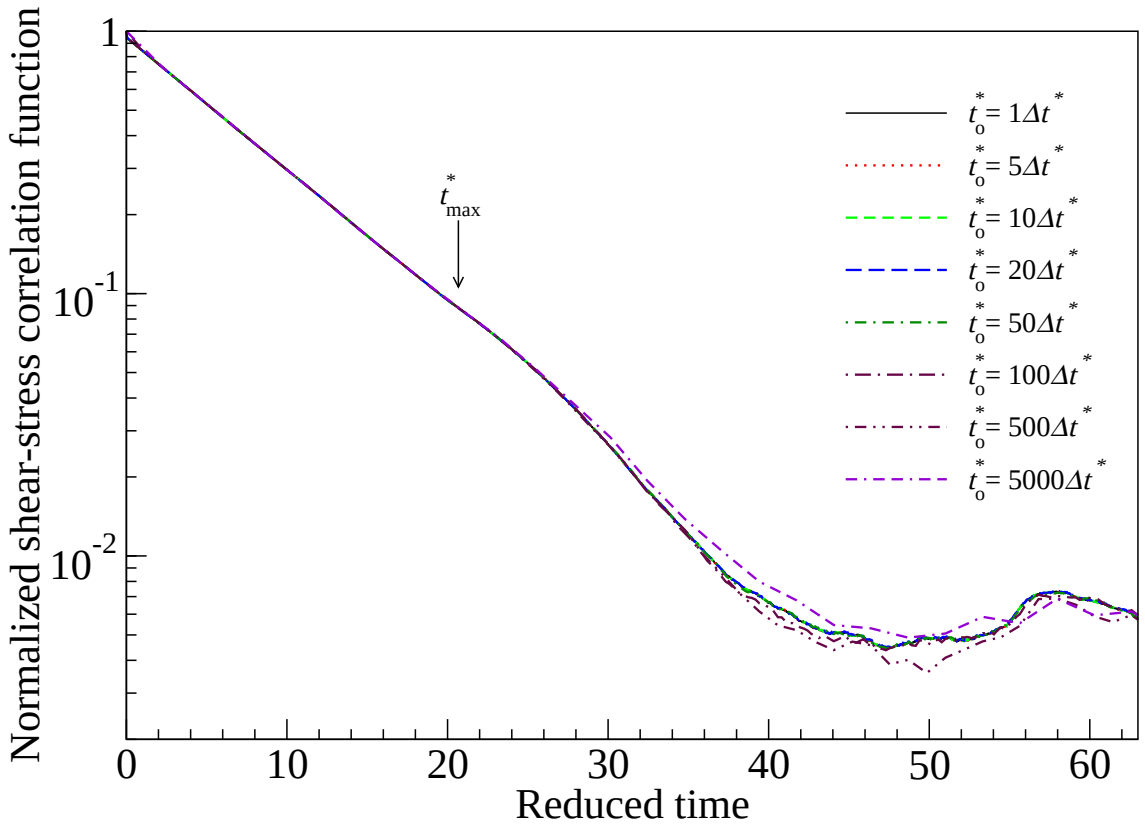

FIG. 2. Effect of time interval between the beginnings of two successive time windows, t_o^*, on calculation of the normalized shear-stress correlation function of LJ fluid at a reduced density of 0.01 and a reduced temperature of 5.0.

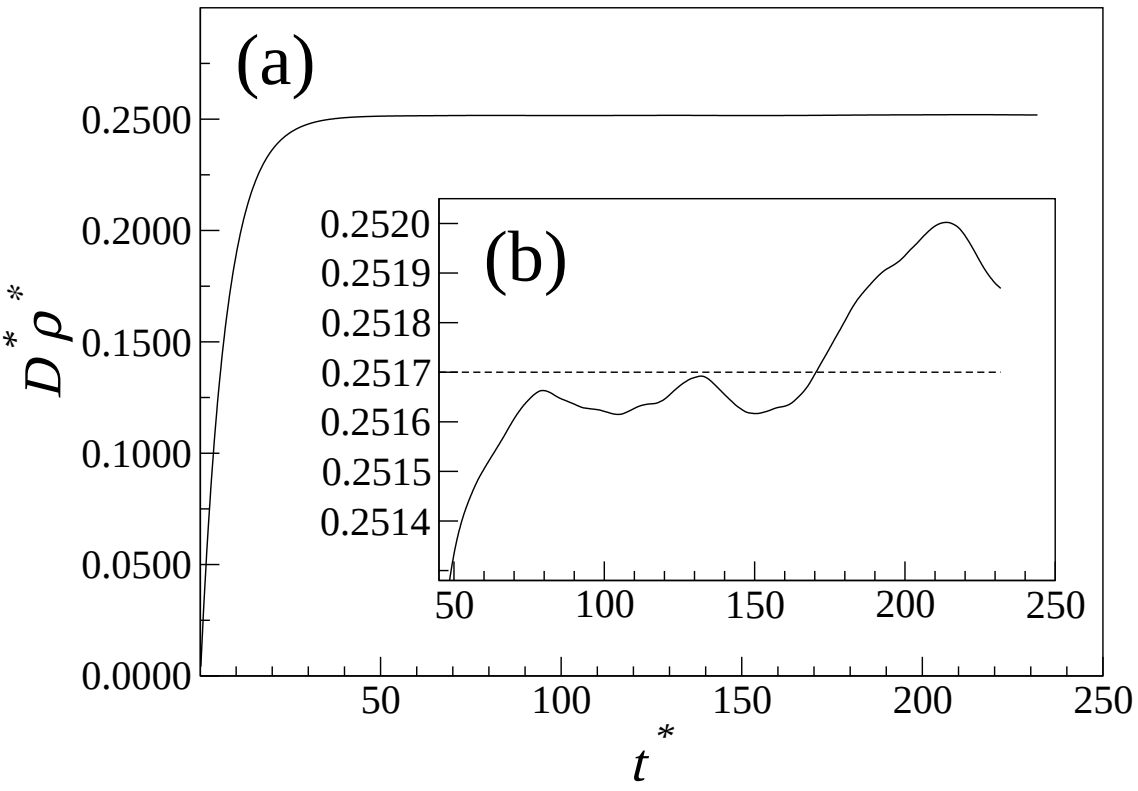

FIG. 3. Reduced self-diffusion coefficient of LJ fluid at a reduced temperature of 1.8 and a reduced density of 0.02 versus time of correlation (a) from zero-time and (b) from decay-time. (Dotted line: mean value.)

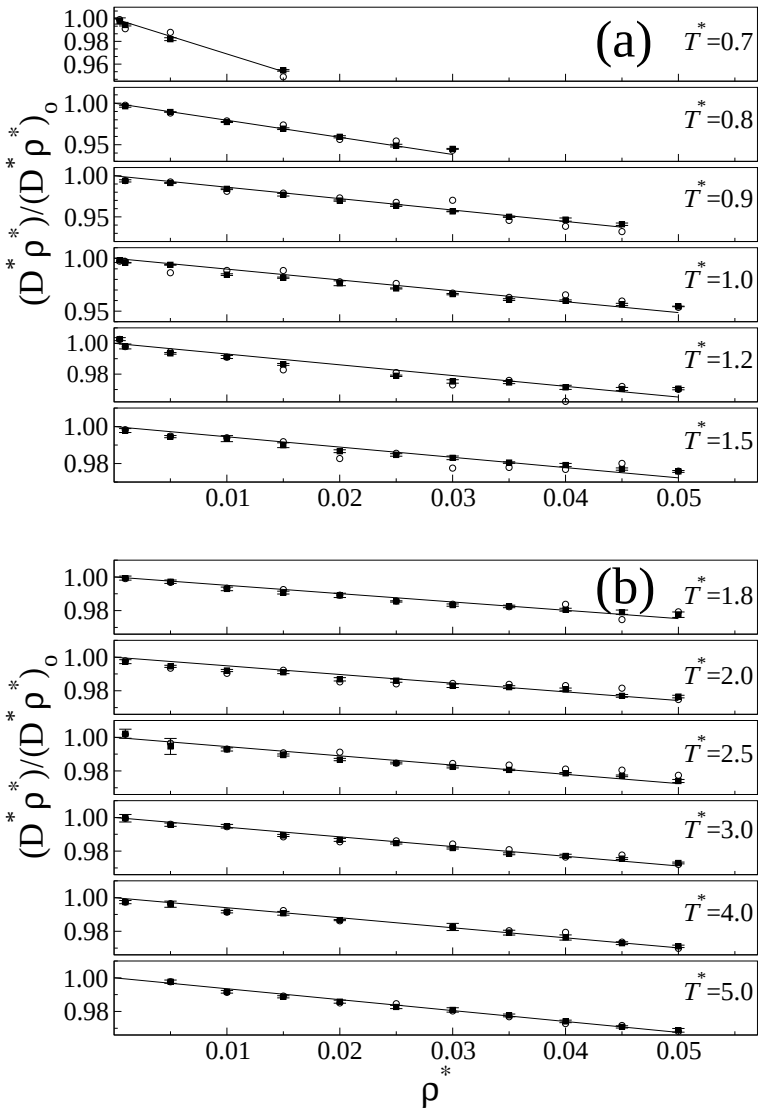

FIG. 4. Density dependence of the simulated reduced self-diffusion coefficients of LJ fluid divided by their values at zero density limit from the Chapman-Enskog theory (a) for isotherms of 0.7 to 1.5 and (b) for isotherms of 1.8 to 5.0. (Filled squares with error bars: temperature corrected values; circles: values at simulated temperatures; solid line: fitted linear regime.)

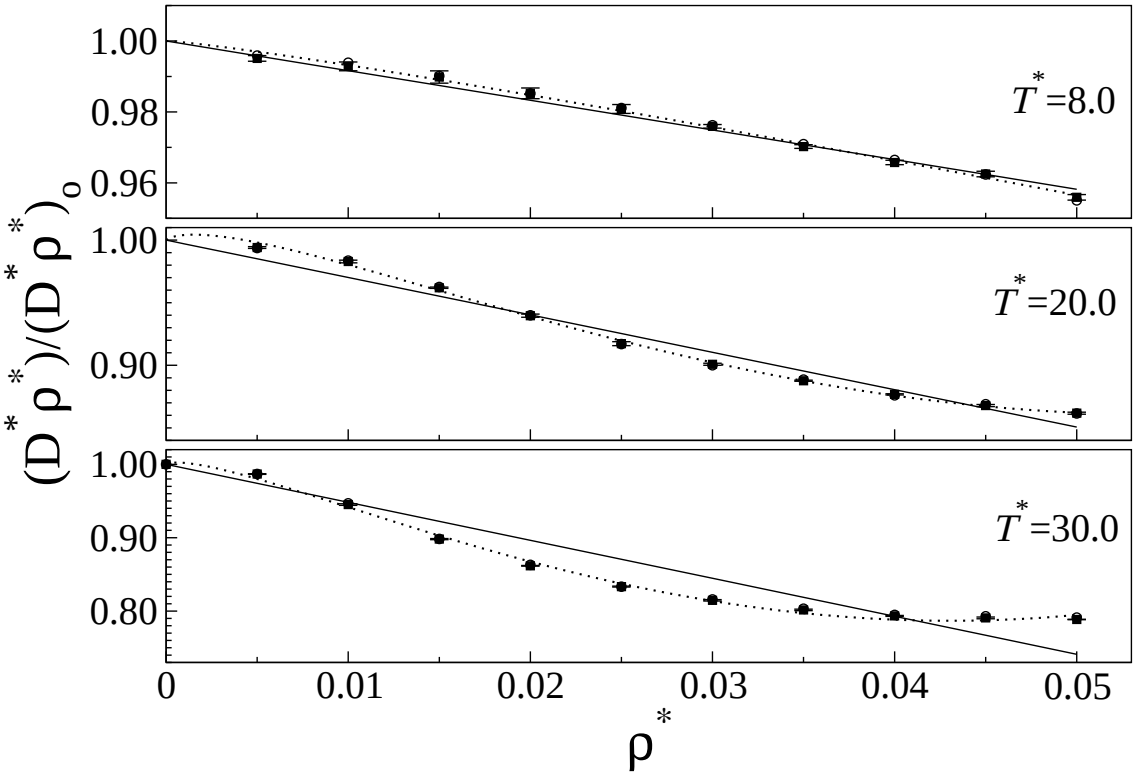

FIG. 5. Density dependence of the simulated reduced self-diffusion coefficients of LJ fluid divided by their values at zero density limit from the Chapman-Enskog theory for isotherms of 8.0, 20.0, and 30.0. (Legend as in FIG. 4; dotted line: fitted up to fourth term of Eq. (1).)

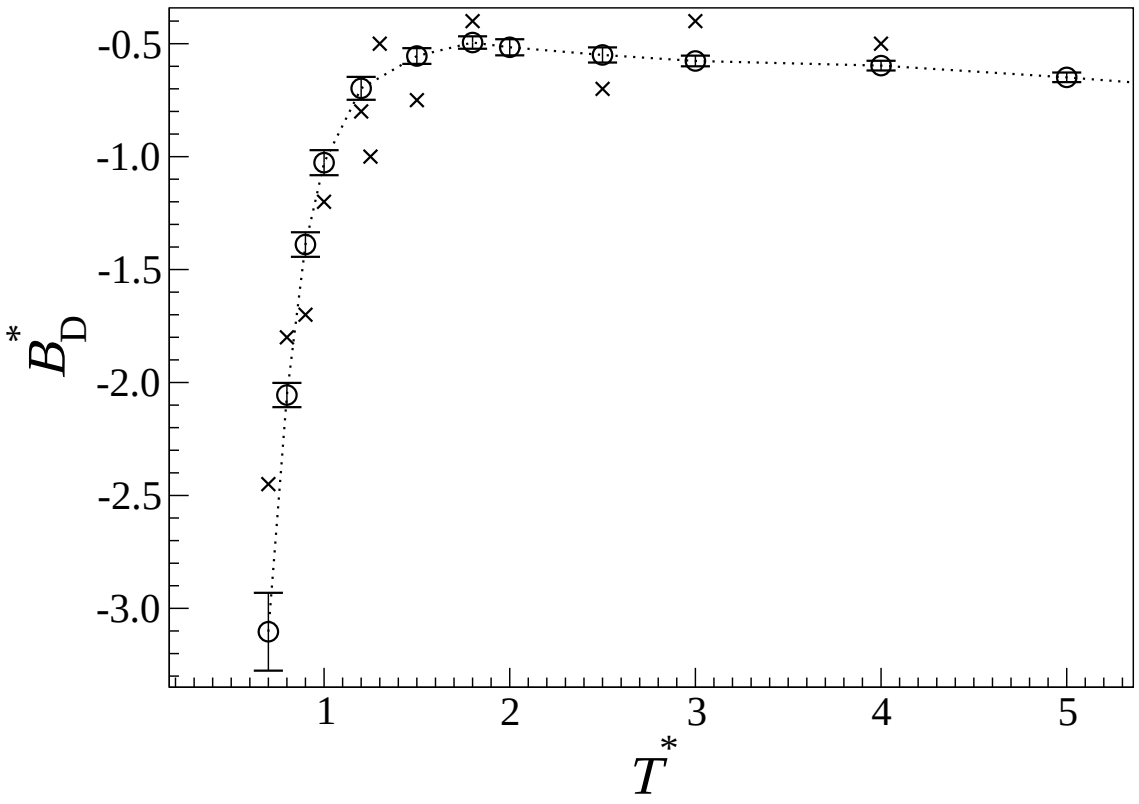

FIG. 6. Second self-diffusion virial coefficients of LJ fluid as a function of reduced temperature. (Circles with error bars: this work; crosses: from Ref. [20].)

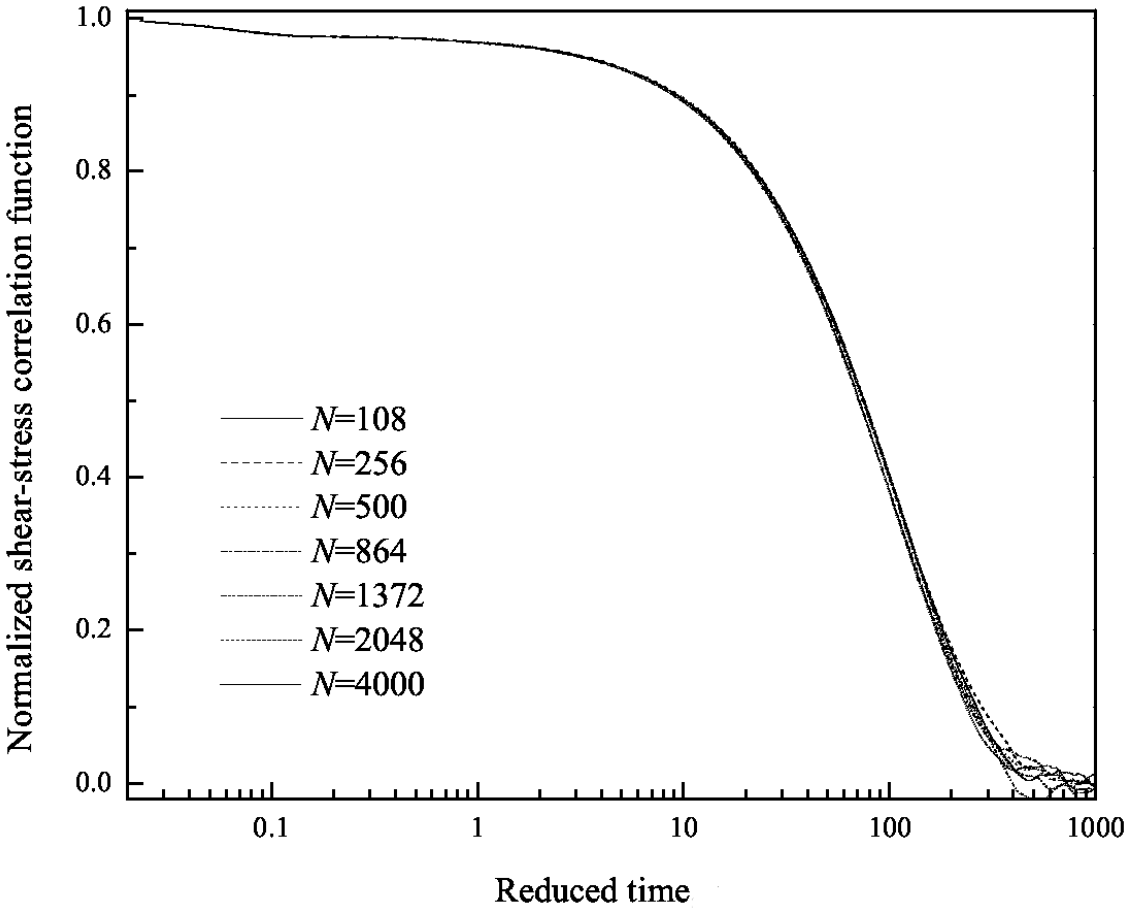

FIG. 7. Normalized shear-stress correlation functions of LJ fluid at a reduced temperature of 1.2 and a reduced density of 0.001 with different numbers of atoms in the simulation primary cell.

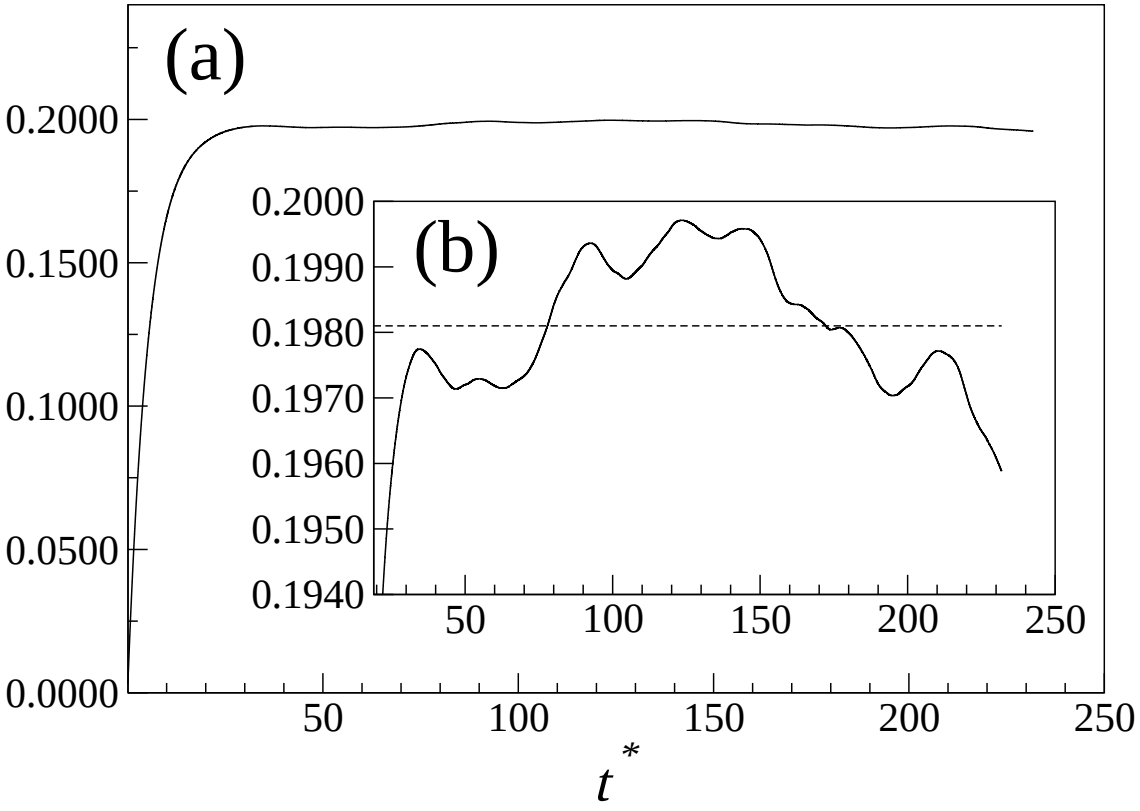

FIG. 8. Reduced viscosity coefficient of LJ fluid at a reduced temperature of 1.8 and a reduced density of 0.02 versus time of correlation (a) from zero-time and (b) from decay-time. (Dotted line: mean value.)

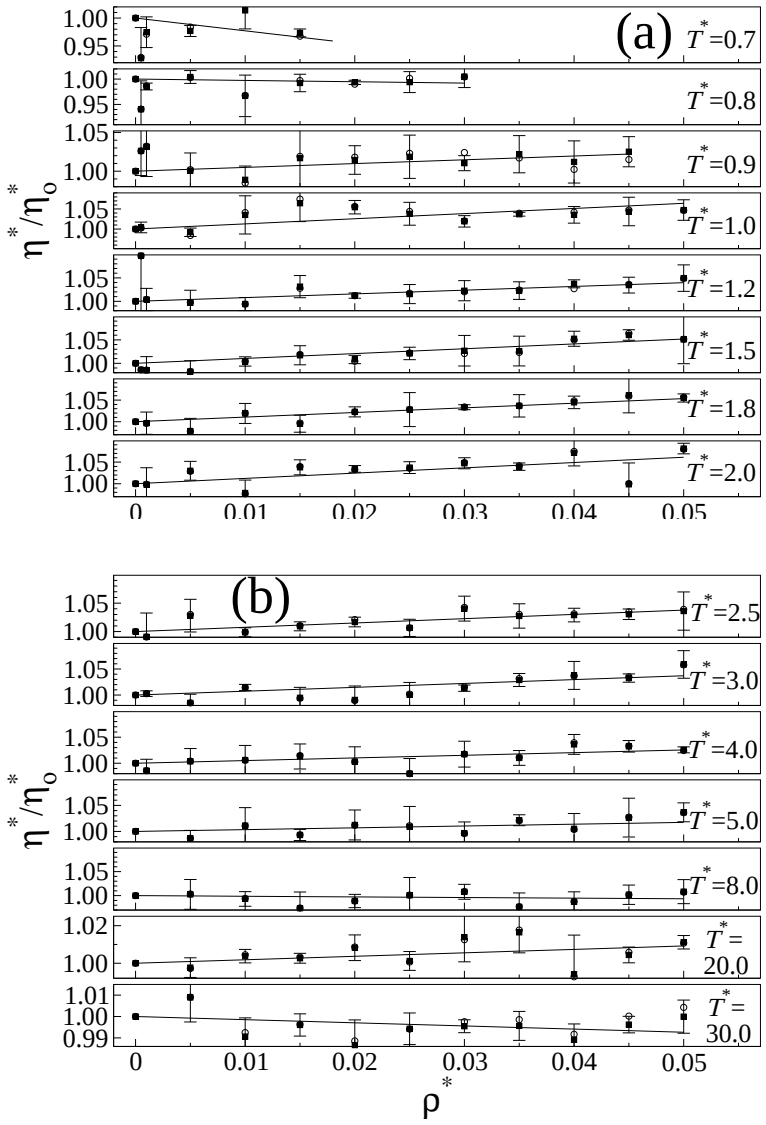

FIG. 9. Density dependence of the simulated reduced viscosity coefficients of LJ fluid divided by their values at zero density limit from the Chapman-Enskog theory (a) for isotherms of 0.7 to 2.0 and (b) for isotherms of 2.5 to 30.0. (Legend as in FIG. 4)

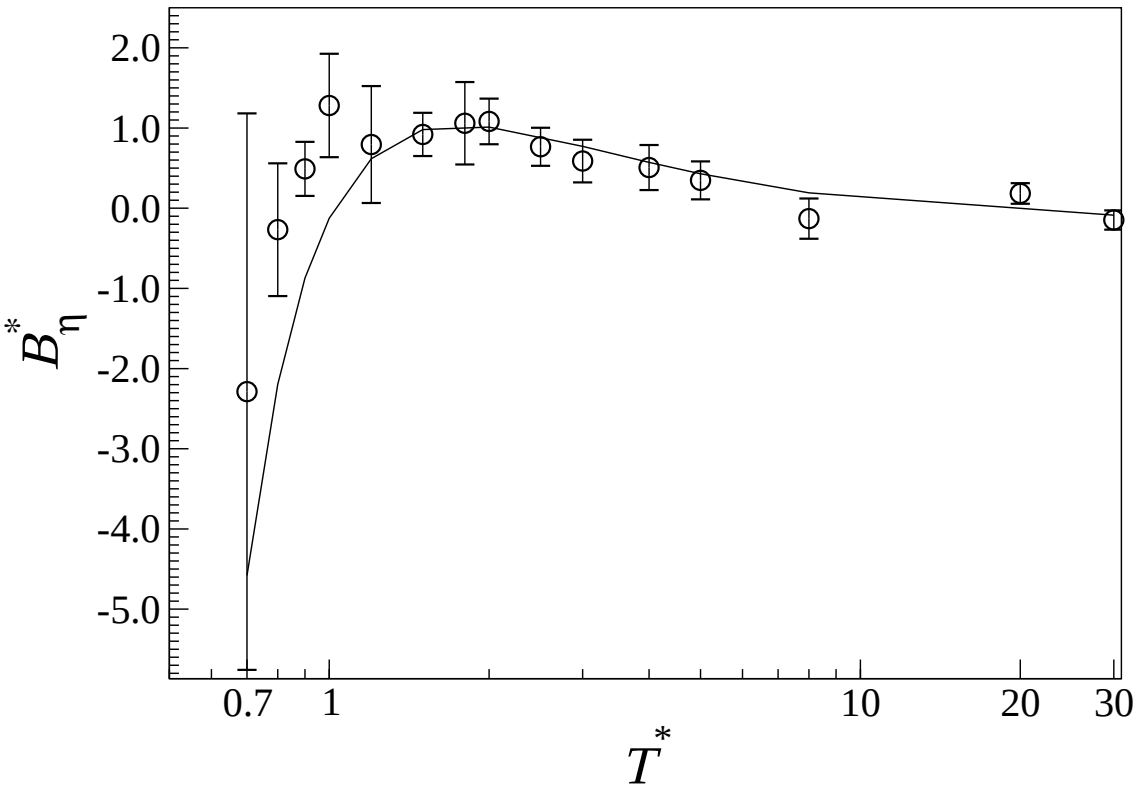

FIG. 10. Second viscosity virial coefficients of LJ fluid as a function of reduced temperature. (Circles with error bars: this work; solid line: Rainwater-Friend theory, Ref. [8].)

TABLE I. Reduced adiabatic compressibility, $\kappa_{\rm s}^*$; reduced speed of sound, $c_{\rm s}^*$; and reduced beginning time of the artificial PBC effect on VACF, $t_{\rm max}^*$, for LJ fluid at $T^* = 1.2$ and $\rho^* = 0.001$, simulated with N particles for the duration of $t^* = 1 \times 10^8$.

N	$\kappa_{\rm s}^*$	$c_{\rm s}^*$	$t_{\rm max}^*$
108	524.2	1.381	34.48
256	507.6	1.404	45.24
500	505.6	1.406	56.44
864	503.2	1.410	67.56
1372	502.8	1.410	79.10
2048	502.3	1.411	90.00
4000	501.6	1.412	112.40

TABLE II. Simulated reduced second self-diffusion virial coefficients, B_{D}^{*}; reduced second viscosity virial coefficients, B_{η}^{*}; and their standard deviations [$SD(B_{\mathrm{D}}^{*})$ and $SD(B_{\eta}^{*})$] for the Lennard-Jones fluid at different temperatures.

T^{*}	B_{D}^{*}	$SD(B_{\mathrm{D}}^{*})$	B_{η}^{*}	$SD(B_{\eta}^{*})$
0.7	-3.103	0.1723	-2.287	3.470
0.8	-2.056	0.0537	-0.268	0.828
0.9	-1.389	0.0543	0.490	0.337
1.0	-1.027	0.0555	1.281	0.645
1.2	-0.698	0.0509	0.794	0.729
1.5	-0.555	0.0348	0.920	0.270
1.8	-0.495	0.0275	1.059	0.514
2.0	-0.516	0.0357	1.082	0.285
2.5	-0.550	0.0335	0.766	0.237
3.0	-0.576	0.0238	0.588	0.266
4.0	-0.597	0.0216	0.507	0.281
5.0	-0.649	0.0212	0.347	0.237
8.0	-0.836	0.0296	-0.130	0.251
20.0	-	-	0.184	0.129
30.0	-	-	-0.147	0.120